ONSET OF LIQUID-METAL MAGNETOCONVECTION IN A CYLINDER

Matthew McCormack
School of Mathematics and
Maxwell Institute for
Mathematical Sciences,
University of Edinburgh,
Edinburgh, UK,
matthew.mccormack@ed.ac.uk

Asif Nawaz
School of Mathematics and
Maxwell Institute for
Mathematical Sciences,
University of Edinburgh,
Edinburgh, UK,
A.Nawaz-1@sms.ed.ac.uk

Andrei Teimurazov
Max Planck Institute for
Dynamics and Self-Organization,
37077 Göttingen, Germany,
andrei.teimurazov@ds.mpg.de

Olga Shishkina
Max Planck Institute for
Dynamics and Self-Organization,
37077 Göttingen, Germany,
Olga.Shishkina@ds.mpg.de

Moritz Linkmann
School of Mathematics and
Maxwell Institute for
Mathematical Sciences,
University of Edinburgh,
Edinburgh, UK,
Moritz.Linkmann@ed.ac.uk

ABSTRACT

Assessing the linear stability of the motionless conducting solution represents one of the few analytically tractable results in magnetoconvection. However, definitive agreement between theory, numerical simulations and experiments has been lacking. Here, we present DNS results of magnetoconvection in a cylinder which capture the linear instability, and the nonlinear solutions which emerge from it. The simulations agree excellently with previous numerical linear stability calculations and allow for comparison between different asymptotic theories. Doing so, we confirm that the motionless state undergoes a supercritical pitchfork bifurcation that leads to steady nonlinear wall mode solutions, which maintain the azimuthal wavenumber of the linear instability. Although the DNS results agree well with the linear theory, there is still discrepancy between the DNS and earlier experiments performed by Xu *et al.* (2023). These discrepancies point towards multiple stable wall mode states and possibly subcritical behaviour, both of which have been already observed in magnetoconvection in a cube (McCormack *et al.*, 2025).

INTRODUCTION

Seminal work of Chandrasekhar (1952) assessed the linear stability of the motionless conducting solution in magnetoconvection (MC), where a layer of fluid is bounded by a hot lower and cold upper plate and subjected to a vertical uniform magnetic field. The relevant control parameters were determined to be the Rayleigh number Ra and the Hartmann number Ha (or equivalently the Chandrasekhar number $Q = Ha^2$)

$$Ra = \frac{\alpha g\, \delta T\, H^3}{\kappa \nu}, \qquad Ha = B_0 H \sqrt{\frac{\sigma}{\rho \nu}} \tag{1}$$

which, relative to viscosity, quantify strength of the thermal driving and the Lorentz force, respectively. Here, α is the thermal expansion coefficient, g is the acceleration due to gravity, $\delta T > 0$ is the temperature difference across the layer of height H, κ is the thermal diffusivity, ν is the kinematic viscosity, B_0 is the strength of the applied magnetic field, and σ is the electrical conductivity. This stability analysis was performed for a flow with horizontal periodicity, obtaining that the threshold for instability Ra_c is raised as the strength of the magnetic field increased, with $Ra_c = O(Ha^2)$ for a variety of kinematic boundary conditions on the upper and lower plates. Reasonable agreement with this result was reported by experiments soon thereafter (Nakagawa, 1955; Jirlow, 1956; Nakagawa, 1957), and then later (Cioni *et al.*, 2000; Aurnou & Olson, 2001), all of which were performed in cylindrical vessels with varied aspect ratios, and therefore, it appeared that consensus regarding the onset of MC had been reached.

However, it has since been realised that particular attention must be paid to the electrical boundary conditions of the vessel's sidewalls, which often have a much lower conductivity than the fluid itself. In the extreme case where the sidewalls are insulating, the Lorentz force must completely vanish at the wall. Resultingly, by continuity of the current density, convection is more easily triggered in thin layers close to the sidewall than in the bulk of the flow, leading to near-onset flow fields consisting of wall-localised coherent structures known as magnetoconvective wall modes (Liu *et al.*, 2018; Zürner *et al.*, 2020) and motionless fluid in the bulk. The appearance of wall modes has been predicted by linear stability analysis for asymptotically large Ha, first by Houchens *et al.* (2002) for cylindrical domains and later for an isolated sidewall by Busse (2008), both observing $Ra_c = O(Ha^{3/2})$. Owing to this scaling exponent, the wall mode instability is expected to be triggered beneath the bulk instability investigated by Chandrasekhar (1952), seemingly in contradiction to the results of the early experiments. Importantly, however, these experimental results relied on temperature measurements taken by probes in the bulk of the domain or on globally averaged quantities - both of which are expected to be insensitive to the wall modes which are confined to sidewall layers of thickness $\sim Ha^{-1/2}$ according to the stability analysis. Despite the wall mode instability being known for more than two decades, definitive agreement between theory, recent experiments and numerical simulations has been lacking (Xu *et al.*, 2023). In this paper, we address this issue for MC in a cylinder.

FORMULATION

To address these uncertainties, we perform direct numerical simulations of magnetoconvection in a cylinder of aspect ratio $\Gamma = D/H$, where D and H are the diameter and height of the cylinder respectively. For an incompressible fluid under the Oberbeck–Boussinesq approximation and in the quasistatic limit (large magnetic diffusivity η limit), the system evolves according to

$$\partial_t \boldsymbol{u} + \boldsymbol{u}\cdot\nabla\boldsymbol{u} + \nabla p = \sqrt{\frac{Pr}{Ra}}\left[\Delta\boldsymbol{u} + Ha^2(\boldsymbol{j}\times\boldsymbol{e}_z)\right] + T\boldsymbol{e}_z, \quad (2a)$$

$$\partial_t T + \boldsymbol{u}\cdot\nabla T = \frac{1}{\sqrt{RaPr}}\Delta T, \quad (2b)$$

$$\nabla\cdot\boldsymbol{u} = 0, \quad \boldsymbol{j} = -\nabla\phi + (\boldsymbol{u}\times\boldsymbol{e}_z), \quad \Delta\phi = \nabla\cdot(\boldsymbol{u}\times\boldsymbol{e}_z), \quad (2c)$$

where $\boldsymbol{u} = [u_r, u_\theta, w]^T$ is the velocity, p the kinematic pressure, T the temperature field, $\boldsymbol{j}$ the current density, and ϕ the electric field potential. The flow is driven by isothermal lower and upper boundaries set to T_+ and T_- respectively, and the applied magnetic field is uniform and orientated vertically in the direction of $\boldsymbol{e}_z$. The control parameters Ra, Ha and $Pr = \nu/\kappa$ appear in equations (2) by consequence of quantities being non-dimensionalised by the height of the layer, the temperature difference $\delta T = T_+ - T_-$, the free-fall velocity $u_{ff} \equiv (\alpha g H \delta T)^{1/2}$, the free-fall time $t_{ff} \equiv H/u_{ff}$, the pressure ρu_{ff}^2 and the applied magnetic field strength. In this case, we fix $Pr = 0.025$, representative of liquid metals such as the Gallium-Indium-Tin alloy commonly used in experiments. To study the full effect of the wall modes we shall consider electrically insulating boundaries $\partial\phi/\partial\boldsymbol{n} = 0$, where $\boldsymbol{n}$ is the vector orthogonal to the surface, and no-slip kinematic conditions on all walls. Similarly, we apply adiabatic sidewall boundary conditions $\partial T/\partial\boldsymbol{n} = 0$. The spatial domain $\Omega \subset \mathbb{R}^3$ is a cylinder $(r,\theta,z) \in [0, D/2]\times[0,2\pi)\times[-H/2, H/2]$ and is resolved on non-uniform grids using the MC extension of Goldfish (Teimurazov *et al.*, 2024), which uses a third-order Runge-Kutta time integration scheme and a fourth-order finite-volume discretisation. In our DNS, we use at least 128 points in both the radial (r) and azimuthal (θ) directions respectively, and 150 points in the vertical (z) direction.

ONSET OF MAGNETOCONVECTION

Equations (2) admit a simple equilibrium solution consisting of motionless fluid $\boldsymbol{u} = \boldsymbol{0}$ and a linear temperature profile $T(z) = -(\delta T/H)z + \bar{T}$, where $\bar{T} = (T_+ + T_-)/2$. The stability of this solution, which will be referred to as the motionless conducting state EQ_m, shall be the main interest of this paper.

Linear stability theory

The linear stability of the motionless state was studied in a laterally periodic layer by Chandrasekhar (1952), who determined that stability threshold for a steady instability was

$$Ra^{(p)} = \frac{\beta^6 + \pi^2\beta^2 Ha^2}{ak^2}, \quad (3)$$

where k is the horizontal wavenumber, $\beta^2 = k^2 + \pi^2$, and a is a parameter that depends on boundary conditions. For free-slip boundaries $a = 1$, but for no-slip conditions a has a more complex dependence on (Ha, k) which has the asymptotic form $a = 1 + O(1/Ha)$ as $Ha \to \infty$. Therefore, the stability results are independent of the kinematic conditions in this limit, and are practically indistinguishable for $Ha \gtrsim 100$. The most unstable wavenumber $k_c = O(Ha^{1/3})$ and thus, the instability leads to domain-filling convection rolls whose horizontal wavelength decreases as the applied magnetic field is increased.

However, in the presence of insulating sidewalls linear stability results point to a wall localised onset mode with a critical Ra which sets in at lower Ra than the bulk instability for high Ha. Busse (2008) investigated this wall mode instability for an isolated sidewall (single vertical wall which is infinite in its horizontal extent). The asymptotic analysis for large Ha determined that a steady instability occurred at

$$Ra^{(w)} = 3\pi^2\sqrt{3\pi/2}\,Ha^{3/2} + O(Ha) \approx 64.27\,Ha^{3/2}. \quad (4)$$

In the direction horizontally-parallel to the sidewall, the critical mode has an $O(1)$ wavenumber ($k_c = \pi\sqrt{2}$), and thus, the horizontal length scale of the rolls are not affected by the magnetic field as in the bulk instability (although the wavelength is still shorter than 2D non-magnetic Rayleigh–Bénard rolls). In the wall-normal direction, the mode decays as $Ha^{-1/2}$ at leading order, and thus, the modes become increasingly wall-localised as Ha is increased.

Houchens *et al.* (2002) performed a variety of linear stability analyses specifically aimed at cylindrical domains. The first was a analytical-numerical hybrid analysis which coupled a numerically discretised bulk and sidewall to an analytic Hartmann layer on the upper and lower boundaries. The second was an asymptotic result for large Ha which was obtained by a matching procedure between a sidewall layer, the Hartmann layer and the bulk flow, leading to a set of linear algebraic equations which are then solved numerically. The hybrid analysis was compared to a full numerical stability analysis (restricted to low Ha due to spatial resolution and computational constraints) at low Ha, and the asymptotic solution was also compared to the hybrid analysis, all with good agreement. The asymptotic analysis gave

$$Ra^{(w)} \approx 66.42\,Ha^{3/2}, \qquad (\Gamma = 1) \quad (5a)$$

$$Ra^{(w)} \approx 67.75\,Ha^{3/2}, \qquad (\Gamma = 2) \quad (5b)$$

which notably, is very close to the ($\Gamma \to \infty$) result provided by Busse (2008) in which domain confinement effects are not present[1]. Furthermore, we note the difference in kinematic boundary conditions on the upper/lower boundaries between the two studies: free-slip in the case of Busse (2008) and no-slip for Houchens *et al.* (2002). This suggests that the wall mode instability, like in the laterally periodic layer, is independent of these upper/lower boundary conditions for large Ha. In the cases investigated by Houchens *et al.* (2002), the most unstable mode $\sim e^{in\theta}$ at large Ha had an azimuthal wavenumber $n = 2$ for $\Gamma = 1$, and $n = 4$ ($n = 5$) for the hybrid (asymptotic) $\Gamma = 2$ analysis.

[1] We note here that previous comparison of these stability results by Xu *et al.* (2023) contained a typographic error in the $\Gamma = 1$ prefactor of the Houchens *et al.* (2002) analysis which led to the results being misrepresented.

Only recently has the full linear stability problem been solved numerically for cylindrical domains over a wide range of parameter space and aspect ratios (Tao *et al.*, 2026). Although it was found that the wall modes may be suppressed by a sufficiently confined geometry (set $\Gamma = O(Ha^{-1/2})$ such that the diameter of the domain is comparable to the wall-normal extent of the wall modes), at aspect ratios larger than this (and $Ha \gtrsim 20$) wall modes dominate the onset mode with an azimuthal wavenumber that depends on Γ and weakly on Ha. A fit for the Ra threshold for instability was provided for $100 \leq Ha \leq 1000$ for $\Gamma = \{1, 2, 3\}$ obtaining

$$Ra^{(w)} \approx (64.9 \pm 0.6)\, Ha^{(1.50\pm0.01)}, \qquad (\Gamma = 1) \qquad (6a)$$

$$Ra^{(w)} \approx (65.0 \pm 0.6)\, Ha^{(1.51\pm0.01)}, \qquad (\Gamma = 2) \qquad (6b)$$

$$Ra^{(w)} \approx (64.4 \pm 0.6)\, Ha^{(1.51\pm0.01)}. \qquad (\Gamma = 3) \qquad (6c)$$

Therefore, the results of these linear stability analyses are all in good agreement.

We note here the independence of these results on Pr which does not formally appear in the linearised system under the assumption of the motionless state undergoes a steady instability (pitchfork bifurcation). The possibility of an oscillatory instability (Hopf bifurcation) is precluded in the laterally periodic analysis provided that the magnetic diffusivity ratio $\eta/\kappa > 1$, and a similar condition is expected for the wall mode instability. This condition is upheld for the liquid metals we consider where typically $\eta/\kappa \gg 1$.

Experiments & simulations

Although a number of experiments have been conducted to measure the onset of magnetoconvection, early experiments used measurement techniques that were unknowingly biased to measure the bulk instability discovered by Chandrasekhar (1952) and insensitive to wall modes. Since the theoretical discovery of the wall mode instability, only a small number of relevant experiments have been conducted. The first experiment to observe wall modes were by Zürner *et al.* (2020), who explored a wide range of parameter space including values of Ra slightly beneath the bulk onset $Ra^{(p)}$. However, experiments aiming to examine the wall mode onset came later, performed by Xu *et al.* (2023). These results were complimented by direct numerical simulations that revealed the three-dimensional structure of the flow (Xu *et al.*, 2023). However, the simulations could only be run for short times, leading to pattern selection differences and defects that differed from the experiments and linear stability theory. Furthermore, conclusive agreement between the simulations, experiments and theory regarding the stability threshold was also lacking. Therefore, further DNS results run for longer times would be useful to clarify the near-onset behaviour.

RESULTS

Linear stability

We focus on a $\Gamma = 2$ cylinder with $Ha = 200$, allowing us to compare with the DNS and experimental results of Xu *et al.* (2023), and begin by assessing the linear stability threshold. We perturb EQ_m with random noise of amplitude 10^{-6} in all fields, close to the stability threshold. We use the DNS to evolve the flow from this initial condition, first seeing a rapid decay of the solution due to the excitation of strongly damped modes by the random noise. The solution then enters a phase of exponential growth/decay, observed in all variables $\sim e^{\lambda t}$ as

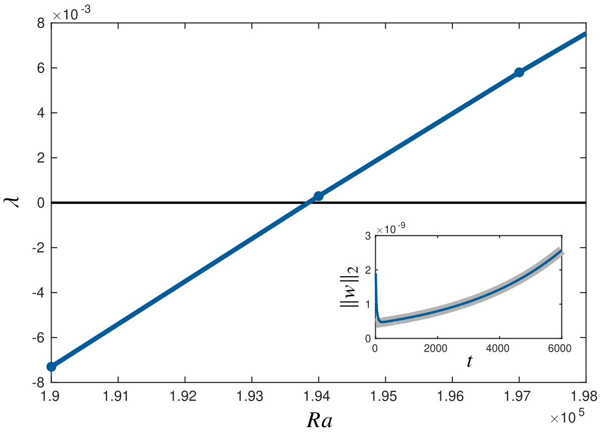

Figure 1. Solution growth rate λ as a function of Ra for $Ha = 200$, $\Gamma = 2$. The inset shows the growth of the 2-norm of the vertical velocity as a function of time at $Ra = 1.94 \times 10^5$. The grey line shows the fit $\|w\|_2 \sim e^{\lambda t}$.

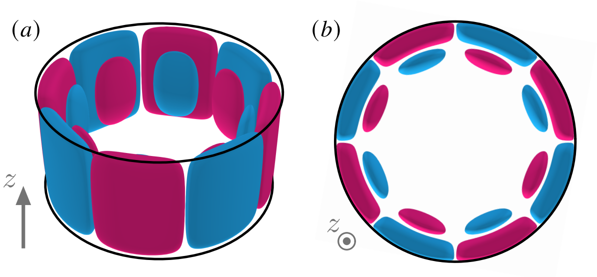

Figure 2. Vertical velocity isosurfaces of the onset mode for $Ha = 200$, $\Gamma = 2$ from a (a) 3D view, and (b) in 2D from above.

expected from the linear dynamics. We determine the growth rate λ as a function of Ra by fitting to the 2-norm of the vertical velocity

$$\|w\|_2 = \left(\int |w(\boldsymbol{x}, t)|^2 \, \mathrm{d}^3\boldsymbol{x} \right)^{1/2}, \qquad (7)$$

although the same growth rate is observed in all variables as expected from linear theory. We plot λ as a function of Ra for cases very close to the linear stability threshold in figure 1, which displays a linear relationship. The curve intersects $\lambda = 0$ at the point of linear instability Ra_c, estimated as $Ra_c \approx 1.9385 \times 10^5$ by our analysis. This instability threshold is in excellent agreement with the numerical linear stability analysis of Tao *et al.* (2026), who reported $Ra_c = 1.94 \times 10^5$ for the same parameter values. The threshold also agrees well with the asymptotic predictions, despite the moderate value of Ha, with the $\Gamma = 2$ prediction of Houchens *et al.* (2002) giving $Ra_c = 1.916 \times 10^5$ ($\approx 1\%$ relative error), and the isolated sidewall prediction of Busse (2008) giving $Ra_c = 1.818 \times 10^5$ ($\approx 6\%$ relative error).

Wavenumber selection

During the phase of exponential growth/decay we observe a wall-localised modal pattern in the flow field with an azimuthal wavenumber $n = 4$ for all cases close to the stability threshold. This modal pattern is shown by vertical velocity isosurfaces in figure 2 for $Ra = 1.94 \times 10^5$. The azimuthal wavenumber of the mode is consistent with the results of Tao

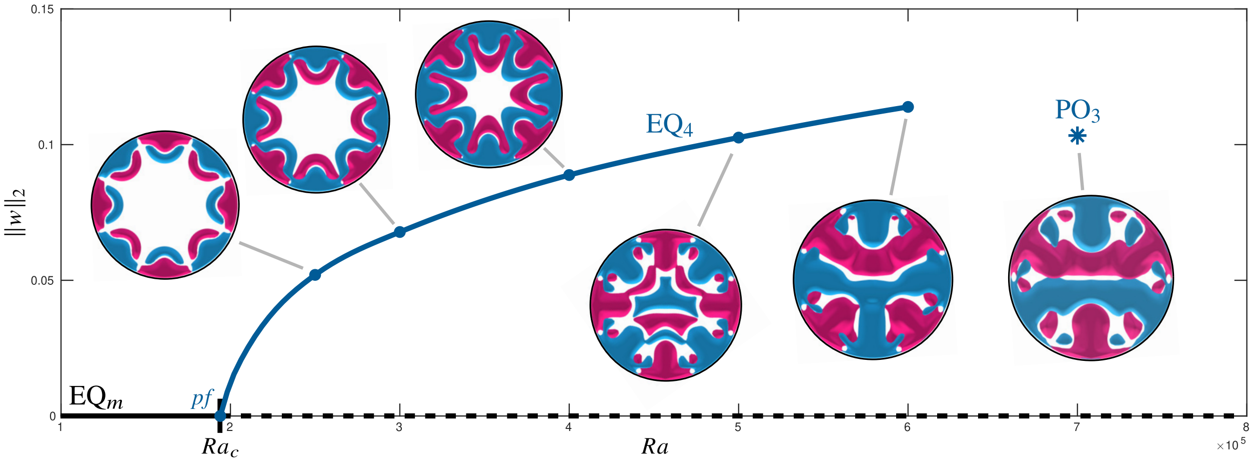

Figure 3. Bifurcation diagram showing the 2-norm of the vertical velocity $\|w\|_2$ for $Ha = 200$, $\Gamma = 2$ of the motionless solution EQ_m (black), the nonlinear branch of 4-mode equilibria (blue), and the stable periodic 3-mode solution (blue star). Stable/unstable solutions are denoted with solid/dashed lines. The corresponding flow field is shown from above using vertical velocity isosurfaces $w = \pm 0.01$ for $Ra < 5\times 10^5$ and $w = \pm 0.02$ for $Ra \geq 5\times 10^5$.

et al. (2026), and the hybrid analysis conducted by Houchens *et al.* (2002). Each wall mode features a two layer wall-normal structure (Liu *et al.*, 2018), which is commonly observed for wall modes in a variety of different geometries.

The dependence of n on Γ has been studied numerically over a wide range of Γ and Ha by (Tao *et al.*, 2026) (see figure 6 therein). However, we note that the observed behaviour can be explained by the asymptotic results of Busse (2008). For an infinitely long sidewall, Busse (2008) found that the critical wall-parallel wavenumber $k_c = \pi\sqrt{2} \approx 4.44$, which is independent of Ha as $Ha \to \infty$. In the cylinder, however, the wavenumber selection is restricted due to the azimuthal periodicity $\theta \in [0, 2\pi)$. Imposing $H = 1$ (without loss of generality), the circumference of the cylinder is $\pi\Gamma$, and therefore, we expect that the azimuthal wavenumber should be selected in a cylinder as

$$n = \lfloor k_c \Gamma/2 \rceil \approx \lfloor 2.22\Gamma \rceil, \tag{8}$$

as $Ha \to \infty$, where $\lfloor\cdot\rceil : \mathbb{R} \to \mathbb{Z}$ denotes rounding to the nearest integer. For $\Gamma = 2$, we obtain $n = 4$ as expected, but furthermore, this relationship accounts well for the wavenumber selection observed by Tao *et al.* (2026) for $Ha \gtrsim 100$ where the dependence on Ha becomes weak. It is worth noting here the close proximity of the $\Gamma = 2$ critical wavenumber to $n = 5$ ($n = \lfloor 4.44\rceil$). The asymptotic results of Houchens *et al.* (2002) for $\Gamma = 2$ predicted $n = 5$ as the critical wavenumber, however, the close proximity to $n = 4$ was acknowledged. With hindsight of knowing Ra_c accurately for this finite value of Ha, it is interesting to note that the asymptotic Ra_c prediction of Houchens *et al.* (2002) is improved by imposing $n = 4$, giving $Ra_c = 1.93\times 10^5$ (< 1% relative error).

Nonlinear regime and symmetries

Having characterised the linear instability, we now progress into the nonlinear regime. Using the motionless state EQ_m as the initial condition, perturbed with random noise of amplitude 10^{-6}, we timestep the DNS code for $Ra = 2.5\times 10^6$ until we obtain a converged nonlinear equilibrium solution. We then use this initial condition and incrementally increase Ra to converge a new equilibrium solution. We iterate this process to obtain a branch of nonlinear equilibrium solutions EQ_4, shown in the bifurcation diagram in figure 3, which inherit the $n = 4$ pattern of wall modes from the linear instability. This is important to distinguish as equivalent DNS simulations run by Xu *et al.* (2023) for shorter simulation times found a pattern defect in the wall modes, giving a wavenumber between $n = 4$ and 5, presumably due to an interaction between the two unstable wavenumbers at relatively small supercriticalities. However, we find that running the simulations for much longer times (many 10s of thermal diffusion times) reveals that this is a transient effect, and that the long-time attractor is a pure $n = 4$ nonlinear wall mode solution.

Having obtained stable nonlinear solutions for $Ra > Ra_c$, we may now characterise the bifurcation associated with the linear instability. The motionless state EQ_m has an $O(2)\times\mathbb{Z}_2$ symmetry: $O(2)$ the symmetry of the disk; and $\mathbb{Z}_2$ coming from the Boussinesq symmetry which gives invariance under $z \mapsto -z$ (with a change in sign $T \mapsto -T$ in the temperature field). However, the bifurcation breaks both the $O(2)$ symmetry resulting in the $n = 4$ wall mode pattern, and the $\mathbb{Z}_2$ symmetry whereby the nonlinear solutions no longer possess the $z \mapsto -z$ Boussinesq symmetry. Since the solution is neutrally stable to changes in its azimuthal orientation, the bifurcation is thus a supercritical circle pitchfork, marked as pf in the bifurcation diagram (figure 3), whereby the amplitude is phase invariant. Therefore the amplitude of the solution near onset has the following normal form

$$\frac{\mathrm{d}A}{\mathrm{d}t} = (\varepsilon - c|A|^2)A, \tag{9}$$

where $\varepsilon = Ra/Ra_c - 1$ measures the supercriticality, and $c > 0$. When $\varepsilon < 0$ only the $A = 0$ solution exists and is stable, corresponding to EQ_m. However when $\varepsilon > 0$, three solutions exist: again $A = 0$ which is now unstable; and $A = \pm\sqrt{\varepsilon/c}$ corresponding to EQ_4. Using the vertical velocity to define the amplitude

$$w(r,\theta,z,t) = \Re[A(t)e^{\mathrm{i}n\theta}\psi(r,z)], \tag{10}$$

where $\psi(r,z)$ describes the radial and vertical structure of the unstable mode (with $\|\psi\|_2 = 1$, thus giving $\|w\|_2 = A$), we measure $c \approx 100$ from the data at $Ha = 200$, although more

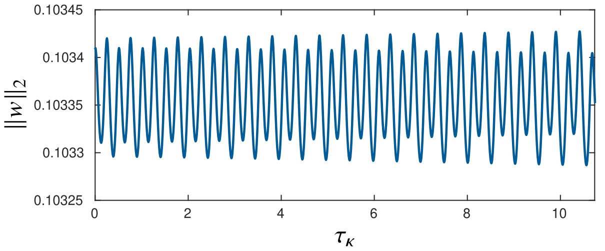

Figure 4. Timeseries of the vertical velocity 2-norm for solution PO_3 at $Ra = 7 \times 10^5$ after a long transient. Time has been renormalised by the thermal diffusion time i.e. $\tau_\kappa = \sqrt{PrRa}\,t$.

equilibria close to onset are required to fit this parameter accurately. Alternatively, c may be calculated through a weakly nonlinear analysis, which is not pursued here (see Vasil *et al.* (2025) for an equivalent calculation in rotating convection).

As EQ_4 is continued to higher Ra, the wall modes begin to grow further into the bulk, maintaining the same symmetry up to $Ra = 4 \times 10^5$. However, increasing Ra to 5×10^5 results in a break in symmetry as a new convection roll appears in the centre of the cylinder between the wall modes (figure 3). Regardless, the solution still maintains the $n = 4$ wall mode pattern. By $Ra = 6 \times 10^5$, the central convection roll has merged with the wall modes, which now stretches across the full horizontal width of the domain, connecting wall modes of the same vertical velocity orientation (figure 3). On increasing Ra to 7×10^5, the flow undergoes a long transient of approximately three thermal diffusion times, before relaxing onto a periodic solution which we will refer to as PO_3, shown in figure 4. The mean flow of this periodic solution is shown in figure 3, which features two domain-wide convection rolls and two wall modes that protrude into the bulk: therefore resulting in a $n = 3$ wall mode pattern. The time dependence in this flow is owed to the two wall mode protrusions which flap back and forth periodically. This kind of flapping behaviour has been seen in MC in a cube across a wide range of parameter values (McCormack *et al.*, 2023, 2025). However, it is worth noting that we do not expect that EQ_4 has undergone a Hopf bifurcation here, as the Hopf bifurcations observed previously typically do not change the number of wall modes in the flow (McCormack *et al.*, 2023, 2025). Rather, it seems likely that changing Ra to 7×10^5 has pushed the initial condition outside the basin of attraction of EQ_4, which may also be unstable by $Ra = 7 \times 10^5$. An investigation of these details shall be presented elsewhere.

Comparison to experiment

The experiments of Xu *et al.* (2023) primarily measure the heat transport in the system averaged in space and time, given in dimensionless form as the Nusselt number

$$Nu = \frac{H}{\kappa \delta T} \langle wT \rangle_{V,t} + 1 \qquad (11)$$

where $\langle \cdot \rangle_{V,t}$ represents the volume and time average. Here, the heat transport is made dimensionless by the heat transport of EQ_m (i.e. by conduction) and thus, $Nu \geq 1$.

From weakly nonlinear theory, Nu is expected to vary with the square of the amplitude A^2, and thus, should be proportional to ε as

$$Nu - 1 = K\varepsilon, \qquad (12)$$

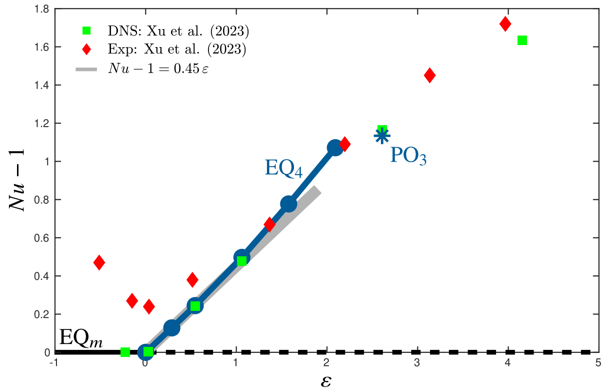

Figure 5. Nu as a function of ε for the solutions shown in figure 3. We compare these to the previous DNS and experimental results of Xu *et al.* (2023). All solutions shown are for $Ha \approx 200$, $\Gamma = 2$.

where K is the convective conductivity. We plot our DNS data against ε in figure 5 and indeed observe a linear relationship close to onset, in this case with $K \approx 0.45$. The numerical values of Nu agree well with the DNS of Xu *et al.* (2023), despite the slight differences in wall mode pattern already discussed.

We now compare the results of these numerical simulations to the experiments of Xu *et al.* (2023), noting that small variations in the magnetic field (less than 5%) exist for the $Ha \approx 200$ data. We account for this by adapting Ra_c in the calculation of ε for each data point, which makes only a minor adjustment in the results. In general, we observe good agreement in the heat transport measurements between experiments and simulations for $\varepsilon \gtrsim 1$. However, the experimental data deviates from the simulations by more than 20% for $\varepsilon < 1$. Furthermore, the experiments exhibit convection ($Nu > 1$) beneath the linear stability threshold ($\varepsilon < 0$), suggesting the possibility of subcritical behaviour. This is notable as subcritical equilibrium solutions, featuring wall modes with longer horizontal wavelengths than the linear instability, have recently been observed in MC in a cube (McCormack *et al.*, 2025). Although the spatial organisation of the wall modes has not been investigated in detail by Xu *et al.* (2023) for this $\varepsilon < 1$ regime, it is interesting to note that the flow reported at $Ra = 2 \times 10^5$ ($\varepsilon \approx 0.04$ with $Nu = 1.24$) features two pairs of wall modes with different horizontal length scales (see figure 3(a) (top) in Xu *et al.* (2023)). This state is reminiscent of the mixed-symmetry branch of solutions (MB) seen by McCormack *et al.* (2025) in a cube, which extended beneath the linear stability threshold and similarly featured a mixture of wide-narrow wall modes coexisting along the sidewalls.

Despite the good agreement with the Nu results of the experiment when $\varepsilon > 1$, the wall mode pattern observed is different than the experiments which exhibit an $n = 3$ pattern for this range of Ra (see figure 3(b, c) (top) in Xu *et al.* (2023)). Only for $Ra = 7 \times 10^5$ have we observed an $n = 3$ pattern, with $n = 4$ being observed for $Ra \leq 6 \times 10^5$. This suggests that multiple wall mode states may be stable close to onset, similar to that observed in the cube by McCormack *et al.* (2025). Preliminary DNS results suggest that multiple stable states do exist and that hysteresis effects are at play in this system, both of which shall be discussed in a later publication.

CONCLUSION

In this paper we have presented DNS results at $Ha = 200$ in a $\Gamma = 2$ cylinder close to the onset of convection. The results display excellent agreement with numerical linear stability analysis (Tao *et al.*, 2026), and various asymptotic (high Ha) linear stability theories (Houchens *et al.*, 2002; Busse, 2008), both in the numerical value of the linear stability threshold and the azimuthal wavenumber ($n = 4$) of the most unstable mode. Furthermore, we move past the linear regime to determine that the linear instability is associated with a supercritical pitchfork bifurcation which leads to stable nonlinear wall mode solutions that maintain the azimuthal wavenumber of the instability. As Ra is increased, the wall modes grow into the bulk of the domain maintaining their 4-mode pattern. Eventually, the bulk of the flow is destabilised and an additional steady convection roll appears in the centre of the domain, which then begins to merge with the wall modes. Only as Ra reaches 7×10^5 do we observe a switch to a 3-mode wall mode pattern, which is accompanied by time-dependent behaviour. The results we obtain in the nonlinear regime provide reasonable agreement with previous DNS (Xu *et al.*, 2023) (considering the short runtimes of these past simulations). However, the results still disagree with experiments, particularly close to onset, which exhibit numerically different heat transport values and even different wall mode patterns in some cases. This discrepancy points strongly towards multistability in this flow and possibly to subcritical behaviour, both of which are features that have been observed previously in a cube (McCormack *et al.*, 2025). Preliminary results suggest that multiple states and hysteresis effects exist in this system, and thus we shall investigate these features in more detail in future work.

REFERENCES

Aurnou, JM & Olson, PL 2001 Experiments on rayleigh–bénard convection, magnetoconvection and rotating magnetoconvection in liquid gallium. *J. Fluid Mech.* **430**, 283–307.

Busse, F H 2008 Asymptotic theory of wall-attached convection in a horizontal fluid layer with a vertical magnetic field. *Phys. Fluids* **20** (2).

Chandrasekhar, S. 1952 XLVI. On the inhibition of convection by a magnetic field. *Lond. Edinb. Dubl. Phil. Mag. J. Sci.* **43** (340), 501–532.

Cioni, S, Chaumat, S & Sommeria, J 2000 Effect of a vertical magnetic field on turbulent Rayleigh-Bénard convection. *Phys. Rev. E* **62** (4), R4520.

Houchens, BC, Witkowski, L Martin & Walker, JS 2002 Rayleigh–Bénard instability in a vertical cylinder with a vertical magnetic field. *J. Fluid Mech.* **469**, 189–207.

Jirlow, K 1956 Experimental investigation of the inhibition of convection by a magnetic field. *Tellus* **8** (2), 252–253.

Liu, W., Krasnov, D. & Schumacher, J. 2018 Wall modes in magnetoconvection at high hartmann numbers. *J. Fluid Mech.* **849**, R21–R212.

McCormack, M., Teimurazov, A., Shishkina, O. & Linkmann, M. 2023 Wall mode dynamics and transition to chaos in magnetoconvection with a vertical magnetic field. *J. Fluid Mech.* **975**, R2.

McCormack, M., Teimurazov, A., Shishkina, O. & Linkmann, M. 2025 Subcritical transition and multistability in liquid-metal magnetoconvection with sidewalls. *J. Fluid Mech.* **1023**, R1.

Nakagawa, Y. 1955 An experiment on the inhibition of thermal convection by a magnetic field. *Nature* **175** (4453), 417–419.

Nakagawa, Y 1957 Experiments on the inhibition of thermal convection by a magnetic field. *Proc. R. Soc. Lond. A. Math. Phys. Sci.* **240** (1220), 108–113.

Tao, X., Zhu, X., Ni, M. & Xie, Y. 2026 Onset and length scales of wall modes in confined magnetoconvection with a vertical magnetic field. *J. Fluid Mech.* **1026**, A41.

Teimurazov, A., McCormack, M., Linkmann, M. & Shishkina, O. 2024 Unifying heat transport model for the transition between buoyancy-dominated and lorentz-force-dominated regimes in quasistatic magnetoconvection. *J. Fluid Mech.* **980**, R3.

Vasil, G M, Burns, K J, Lecoanet, D, Oishi, J S, Brown, B & Julien, K 2025 Rapidly rotating wall-mode convection. *J. Fluid Mech.* **1017**, A37.

Xu, Y., Horn, S. & Aurnou, J. M. 2023 Transition from wall modes to multimodality in liquid gallium magnetoconvection. *Phys. Rev. Fluids* **8**, 103503.

Zürner, T., Schindler, F., Vogt, T., Eckert, S. & Schumacher, J. 2020 Flow regimes of Rayleigh–Bénard convection in a vertical magnetic field. *J. Fluid Mech.* **894**, A21.